Hindawi Publishing Corporation
Journal of Atomic, Molecular, and Optical Physics
Volume 2012, Article ID 236793, 11 pages
doi:10.1155/2012/236793

Research Article

Polymorphism, Hydrogen Bond Properties, and Vibrational Structure of 1H-Pyrrolo[3,2-*h*]Quinoline Dimers

Alexandr Gorski,[1] Sylwester Gawinkowski,[1] Roman Luboradzki,[1] Marek Tkacz,[1] Randolph P. Thummel,[2] and Jacek Waluk[1]

[1] *Institute of Physical Chemistry, Polish Academy of Sciences, Kasprzaka 44/52, 01-224 Warsaw, Poland*
[2] *Department of Chemistry, University of Houston, Houston, TX 77204-5003, USA*

Correspondence should be addressed to Jacek Waluk, waluk@ichf.edu.pl

Received 29 February 2012; Accepted 30 May 2012

Academic Editor: Paul Blaise

Two forms of cyclic, doubly hydrogen-bonded dimers are discovered for crystalline 1H-pyrrolo[3,2-*h*]quinoline, a bifunctional molecule possessing both hydrogen bond donor and acceptor groups. One of the forms is planar, the other is twisted. Analysis of IR and Raman spectra, combined with DFT calculations, allows one to assign the observed vibrations and to single out vibrational transitions which can serve as markers of hydrogen bond formation and dimer structure. Raman spectra measured for samples submitted to high pressure indicate a transition from the planar towards the twisted structure. Formation of intermolecular hydrogen bonds leads to a large increase of the Raman intensity of the NH stretching band: it can be readily observed for the dimer, but is absent in the monomer spectrum.

1. Introduction

In studies of the intermolecular hydrogen bond (HB), an important class of model compounds consists of molecules which can form both H-bonded dimers and complexes with water or alcohols [1]. Such molecules are usually characterized by the simultaneous presence of HB donor and acceptor groups. Whether the strength of the intermolecular HBs is greater for dimers or complexes depends on the relative positions of the donor and acceptor in the molecular frame. Interestingly, different structures and stoichiometries are often encountered for the same molecule. A well-known example is 7-azaindole (7AI, Figure 1), which forms doubly hydrogen bonded dimers in solution [2], while the X-ray data reveal a tetrameric structure in the crystalline state [3]. Different stoichiometries and structures are possible for the complexes of 7AI with methanol and water: 1 : 1, 1 : 2, and 1 : 3 species have been detected [4–9].

The crystal structure of multiply H-bonded dimers/oligomers seems to be determined by the interplay of H-bonding and longer range intermolecular interactions. For instance, 1-azacarbazole (1AC), a molecule closely related to 7AI, exists in the crystal in the form of planar, doubly hydrogen bonded dimers [10] (Figure 2). While there is no doubt that 1AC also forms dimers in solutions, various possible structures have been discussed [11–14].

1H-pyrrolo[3,2-*h*]quinoline (PQ, Scheme 1) can be considered a counterpart to 7AI with regard to intermolecular HB characteristics. The NH group of PQ (HB-donor) and the pyridine nitrogen (HB-acceptor) are positioned three bonds apart, whereas in 7AI these groups are separated by two bonds. This change results in completely different excited state behaviour of complexes with water or alcohols [15–20]. Rapid photoinduced double proton transfer is observed for PQ in complexes of 1 : 1 stoichiometry. The process occurs on the time scale of single picoseconds and is not stopped by lowering of temperature or by increasing the viscosity of the medium. On the contrary, the reaction is slower and viscosity-dependent in 7AI complexes [21], since it requires a solvent rearrangement around an excited chromophore [22–27]. These different phototautomerization

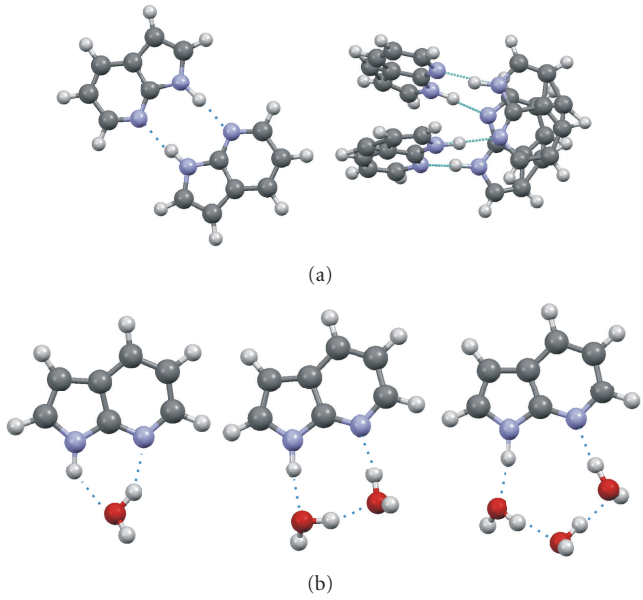

Figure 1: Various motifs of intermolecular HB formed by 7-azaindole. (a) Dimers and tetramers, (b) complexes with water.

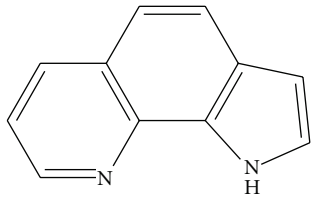

Scheme 1

characteristics reflect different intermolecular HB strengths, imposed by molecular structure.

The HB characteristics, and, in consequence, tautomerization abilities in the dimeric species are expected to become reversed in PQ and 7AI. For the latter, a planar dimeric structure reveals two strong, linear, equivalent HBs. Therefore, it is not quite surprising that photoinduced double proton transfer in 7AI dimers has been observed at temperatures as low as 4 K [28]. In contrast, PQ dimers are predicted by theory to be nonplanar. This has been confirmed by X-ray studies, which reported an angle of 22.6° between the two monomeric units [29]. Our previous work on a similar structure, dipyrido[2,3-*a*:3,2-*i*]carbazole [30] demonstrated that in the crystalline phase this molecule forms cyclic, but strongly nonplanar doubly hydrogen-bonded dimers (Figure 3). No tautomeric fluorescence has been observed for such a dimer, but it could be readily detected when the crystalline sample was exposed to water vapor, prepared on a hydrophilic support, or embedded in a polymer containing hydroxyl groups. A general conclusion from this study was that HB-donor-acceptor molecules which readily form flat dimers should have a weak tendency for the formation of cyclic complexes, and *vice versa*.

In this work, we analyze structure and vibrational spectra of crystalline PQ dimers. Somewhat unexpectedly, our X-ray

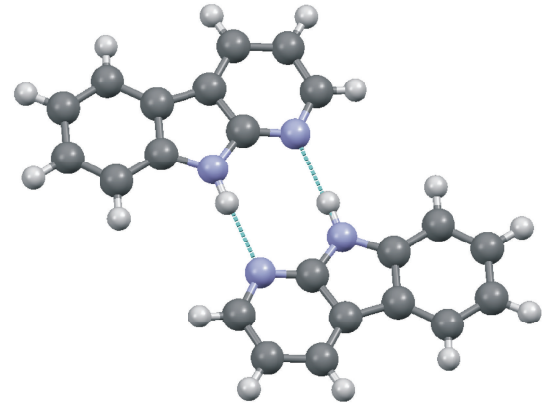

Figure 2: The structure of dimers of 1-azacarbazole in the solid phase.

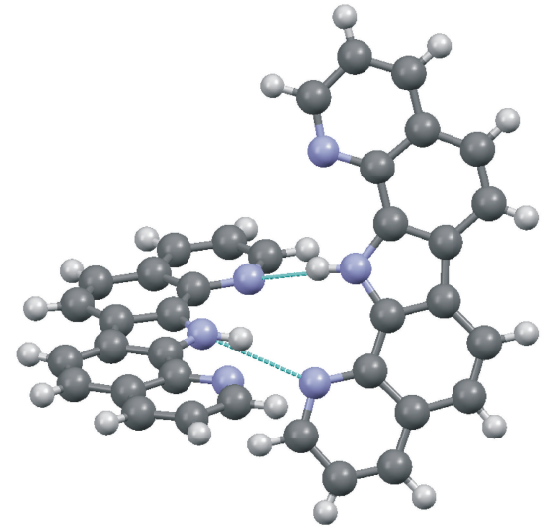

Figure 3: The X-ray structure of dipyrido[2,3-*a*:3,2-*i*]carbazole.

measurements of PQ reveal the existence of planar, doubly hydrogen-bonded dimeric species, and thus a structure very different than the one reported previously [29] (Figure 4). We analyze the experimental and theoretically predicted vibrational patterns, with particular interest regarding the vibrations involved in intermolecular hydrogen bonds. Finally, we show the influence of high pressure upon the HB strength, manifested by spectral shifts observed in the Raman spectra.

2. Experimental and Theoretical Details

Synthesis and purification of PQ have been described before [31].

The IR spectra were recorded on a Nicolet Magna 560 FTIR spectrometer, equipped with MCT/B liquid-nitrogen-cooled detector, with 1 cm^{-1} resolution. For the measurements of infrared spectra, thin polycrystalline PQ films were prepared on KBr or ZnSe windows by quick evaporation from a concentrated solution. The monomer IR

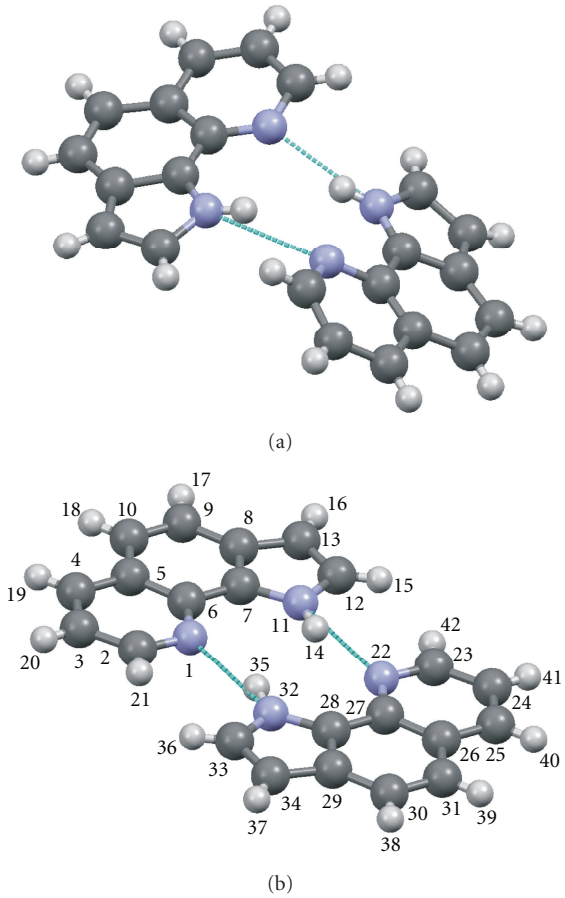

FIGURE 4: (a) X-ray structure of PQ reported in [29]; the geometrical positions of hydrogen atoms were inserted. (b) Our X-ray structure and atom numbering.

spectra have been recorded for PQ isolated in argon matrices using a closed-cycle helium cryostat (CSW-202N, Advanced Research Systems). The compound, contained in a glass tube, was heated to 350 K and codeposited with argon at a ratio of about 1 : 1000 onto a cold (20 K) KBr window mounted in a cryostat with 10^{-6} Torr background pressure. During spectral measurements the matrix temperature was kept at 10 K.

Renishaw inVia microscopic system was used for the measurements of Raman spectra. Ar^+ 514.5 nm (Stellar Pro Modu-Laser, LLC) laser line and a diode laser (HPNIR785) emitting 785 nm line were used as the excitation sources. With a ×100 microscope objective the laser light was focused on a sample, the laser power at the sample being 5 mW or less. The Raman scattered light was collected by the same objective through a cut-off filter to block out Rayleigh scattering. Gratings of 1800 and 1200 grooves/mm were used for 514.5 and 785 nm laser lines, respectively. The resolution was 5 cm^{-1}, with the wavenumber accuracy of 2 cm^{-1}, both calibrated with the Rayleigh line and the 520.6 cm^{-1} line of silicon. The Raman scattered light was recorded by a 1024 × 256 pixel Peltier-cooled RenCam CCD detector.

High pressure experiments have been performed in Takemura type of diamond anvil cell [32]. The diameter of the diamond culet was 600 μm and a gasket made of stainless steel was used with 300 μm centrally drilled hole. Sample powder was loaded into the gasket hole without any pressure transmitting medium. Pressures were measured by recording the fluorescence spectrum of a small ruby chip embedded in the sample and converting the shift of the wavelength of the R_1 line to pressure, according to the scale proposed by Mao [33].

The samples of different polymorphs were prepared by quick crystallization by evaporation from concentrated PQ solutions in dichloromethane, diethyl ether, methanol, cyclohexane, and toluene.

For the X-ray studies, a colorless PQ crystal of approximate dimensions of 0.1 × 0.2 × 0.2 mm^3 was used. Diffraction data were collected at 100 K using a Bruker Kappa CCD diffractometer with graphite monochromated Mo Kα radiation. Structure was solved by direct methods (SHELXS-97) and refined on F^2 by full-matrix least-squares method (SHELXL-97) [34]. Formula is $C_{11}H_8N_2$, monoclinic, space group $P2_1/c$, $a = 9.0104(4)$, $b = 4.7302(1)$, $c = 19.3117(9)$ Å, $\beta = 103.1825(17)^\circ$, $R_1 = 0.0449$ ($I > 2\sigma(I)$), $wR_2 = 0.1144$ for all data.

Unit cell parameters (but not the whole data) were also measured at room temperature, showing no significant differences compared with 100 K data ($a = 9.13$, $b = 4.87$, $c = 19.42$ Å, $\beta = 102.54^\circ$, parameters not refined).

The crystallographic data have been deposited with the Cambridge Crystallographic Data Centre as a supplementary publication no. CCDC 868707. The data can be obtained free of charge at http://www.ccdc.cam.ac.uk or from the Cambridge Crystallographic Data Centre, 12 Union Road, Cambridge CB2 1EZ, UK.

Geometry optimizations were performed using density functional theory (DFT), with B3LYP functional and cc-PVTZ basis set, as implemented in Gaussian 09. This choice of functional/basis set was guided by extensive calculations for the PQ monomer which resulted in reliable assignments of nearly all of the vibrations.

In order to simulate the structure of PQ dimers in the crystalline environment, DFT-based quantum chemical calculations were performed using the CASTEP (Cambridge Serial Total Energy Package) computer code [35] in the framework of the generalized gradient approximation (GGA), as proposed by Perdew et al. [36], in combination with Vanderbilt ultrasoft pseudopotentials [37]. The plane wave basis set was truncated at a kinetic energy of 240 eV. Computations were performed over a range of k-points within the Brillouin zone as generated by the full Monkhorst-Pack scheme [38] with a 2 × 2 × 1 mesh. A further increase of the cutoff energy and the number of k-points resulted in negligibly small changes in structure energies, indicating that the energy values are well converged. Two initial geometries of planar and twisted PQ dimers were taken from the X-ray data. In every case a slab including 16 molecules of PQ was constructed and repeated periodically.

3. Results

3.1. Dimer Structure. Geometry optimization performed for the PQ dimer yields a nonplanar, doubly H-bonded structure. The calculated nonplanar geometry agrees qualitatively with the X-ray data published in 1991 (Figure 4(a)). However, the quantitative differences are quite significant. The calculated twisting angle between the monomeric moieties, 45.6°, is much larger than the experimental one, 22.6°. For the separation of the H-bonded nitrogen atoms, the same value, 2.98 Å, is computed for both pairs, while the reported X-ray distances are very different, 2.92 and 2.99 Å. The calculations yield nearly planar monomeric units in the dimer, whereas the experiment clearly shows distortions. For instance, the experimental NCCN angles are 3.8° and 5.4°, while the calculations yield the same, smaller value of 2.5°. These results suggest that intermolecular interactions in the crystal may affect the dimer structure. We have therefore repeated the X-ray measurements, performing experiments both at 293 K and at lower temperatures. Surprisingly, a different structure than previously reported was obtained (Figure 4(b)), consisting of two doubly H-bonded PQ monomeric units in a planar arrangement. In order to obtain a theoretical model for the planar dimer, we imposed the planarity in the optimization procedure. This resulted in one negative frequency in the optimized structure, the vibration corresponding to mutual twisting of the planar moieties. Computationally, the planar geometry shows the NN distance of 3.12 Å, whereas the experimental value is 3.01 Å.

One can conclude that PQ forms polymorphs in the crystal, which differ in the structure of dimers, especially with regard to parameters usually considered important for the strength of intermolecular hydrogen bond. Therefore it seemed interesting to carry out vibrational spectroscopy studies in order to (i) determine how does the formation of a doubly H-bonded dimer affect the vibrational pattern and (ii) probe the possible differences in the vibrational structure between planar and nonplanar (but both doubly H-bonded) dimers.

3.2. IR Measurements. Figure 5 presents the IR spectra recorded for the monomeric PQ isolated in an Ar matrix and the spectra of polycrystalline PQ, corresponding to the planar dimeric structure, measured on a KBr window. The experimental data are compared with the results of calculations performed for the monomer and for the two forms of the dimer: a fully-optimized non-planar structure and a form with imposed planar geometry.

The spectra of monomeric PQ are very well reproduced by calculations with regard to both band positions and intensities. They will be treated in detail in a separate work, in which the combination of theoretical modelling, IR, Raman, and high resolution fluorescence spectra obtained for supersonic jet-isolated PQ allowed reliable assignments of nearly all of 57 vibrations of monomeric PQ. Here, we focus on the dimer, using the monomer vibrations as a starting point. Figure 5 shows that, while the general pattern of the IR spectrum of dimeric PQ roughly resembles that

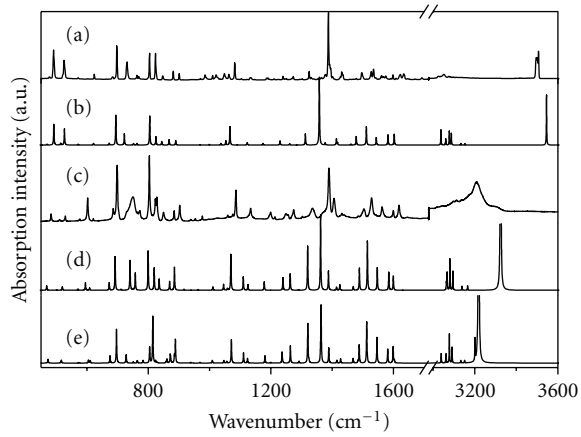

Figure 5: (a) IR spectrum of the monomer in Ar matrix at 15 K; (b) simulated monomer spectrum; (c) dimeric, polycrystalline PQ at 293 K; results of calculations performed for the planar (d) and twisted (e) dimer. The scaling factor of 0.9682 was used in calculations.

of the monomer, significant differences are observed in specific regions. The largest difference is observed for the NH stretching mode. The monomer peak observed around 3500 cm^{-1} (the observed triplet is due to argon site structure) disappears in the crystalline sample, where a broad band is detected, centered at 3210 cm^{-1}. This red shift of almost 300 cm^{-1} is characteristic for the formation of fairly strong NH$\cdots$N intermolecular hydrogen bonds. The calculations predict the shifts of 320 and 220 cm^{-1} for the twisted and planar forms, respectively. As expected, the larger shift is computed for a structure with a shorter N–N distance, and thus a stronger hydrogen bond. The better agreement with experiment for the larger value is somewhat misleading, since the X-ray measurements demonstrated that the sample corresponded to a planar dimer. Further arguments are provided by the analysis of the IR spectrum in the energy region corresponding to out-of-plane vibrations. For the monomeric PQ, calculations yield two modes that contain significant NH out-of-plane contributions. They can be readily identified in the experimental spectrum as the bands at 491 and 527 cm^{-1}. In the IR spectrum of a dimer these bands are still observed, but, in addition, a broad band appears at 743 cm^{-1}, in nice agreement with calculations, which predict for a planar structure a transition at 734 cm^{-1}. For the twisted dimer structure, there no longer exist pure "out-of-plane" modes. The mode which still retains much of that character is predicted to lie at 807 cm^{-1} and to have an intensity twice that of the planar structure. Comparison of the experimental and simulated IR spectra in the region of 650–950 cm^{-1} leaves no doubt that the observed spectrum originates from a planar species. The value of the blue shift of the NH out-of-plane bending mode, which exceeds 200 cm^{-1}, again points to a strong intermolecular HB in dimeric PQ.

There is no single particular vibration in the monomer which could be assigned to a pure NH in-plane bending mode. This is also true for the dimer. The IR transitions

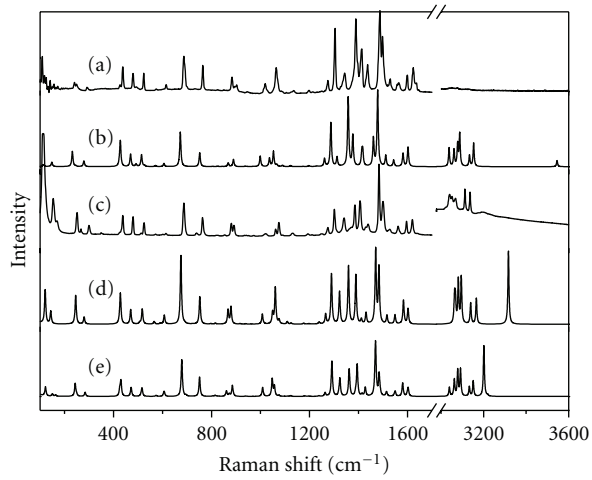

Figure 6: (a) Raman spectrum of the monomer in Ar matrix at 15 K; (b) simulated monomer spectrum; (c) dimeric, polycrystalline PQ, measured at 293 K; results of calculations performed for the planar (d) and twisted (e) dimer. The scaling factor of 0.9682 was used in calculations.

computed for the planar dimer consist of symmetric and antisymmetric combinations of the monomer modes. Only the latter are IR-active. A very similar pattern of IR transitions is obtained for the nonplanar dimer. Figure 5 shows that in the region above 1000 cm^{-1} the predicted IR spectra for both planar and twisted dimer are almost identical.

The analysis of the IR spectra demonstrates that both NH stretching and out-of-plane bending modes are efficient markers for the HB formation. However, only the latter can be used to indicate the planar structure of the H-bonded dimer.

3.3. Raman Spectra. Comparison of Raman spectra simulated and measured for monomeric and dimeric PQ is presented in Figure 6. Contrary to the case of the IR spectra, the calculations now predict differences between monomeric and dimeric species in the region above 1200 cm^{-1}. Below that value, the simulated spectra are very similar for the three species. But even above 1200 cm^{-1}, the Raman spectra computed for planar and twisted dimers resemble each other very strongly, excluding their use for structure determination.

The calculations predict that the Raman activity of the NH stretching mode should be drastically increased, about 15 times, upon HB formation. This increase was confirmed by experiment. No band corresponding to the NH stretch was observed for monomeric PQ, but it could be readily detected at 3200 cm^{-1} for the crystalline sample. Thus, formation of the intermolecularly H-bonded dimer enhances the polarizability to a degree that enables observation of a vibrational feature characteristic of the hydrogen bond.

3.4. Vibrational Assignments. Based on IR and Raman spectra and the results of calculations, we present in Table 1 the tentative assignments for the vibrations of dimeric PQ. The experimental data given in the Table correspond to the planar structure, whereas the calculations are given for both planar and twisted forms. Since the planarity was artificially imposed in the calculations, one might expect that the results in this case are less reliable. Still, as can be seen from Figures 5 and 6, the calculated vibrational patterns are very similar, both for IR and Raman spectra. The largest differences are observed for the NH stretching and out-of-plane bending modes, which were specifically discussed above.

3.5. Obtaining Different Polymorphic Forms. As already mentioned, the crystalline samples of PQ which we have examined by X-ray, IR and Raman techniques corresponded to planar dimers, and thus to a different polymorphic form than observed previously [29]. We have tried to obtain both forms by crystallization from different solvents, and then using Raman spectroscopy as a tool for structure determination. A trial and error approach was adopted, since no information about crystallization details was given in the work reporting the twisted structure [29]. Figure 7 presents the Raman spectra measured for samples crystallized from five different solvents. The spectra are similar, but significant differences can be detected in two regions. A peak of weak intensity appears at 738 cm^{-1} for PQ crystallized from cyclohexane, toluene, and methanol, but not from diethyl ether and dichloromethane. The second region corresponds to two fairly strong peaks observed at 1062 and 1074 cm^{-1}. Their relative intensity patterns (a more intense feature lying at higher energy) are the same for the samples revealing the 738 cm^{-1} transition. For two other samples, which lack the 738 cm^{-1} peak, the intensity ratio changes: now the lower energy peak becomes higher. Such behavior strongly suggests that the PQ samples obtained from cyclohexane, toluene, and methanol correspond to planar dimers, whereas those crystallized from diethyl ether and dichloromethane, to the nonplanar ones. This is confirmed by the results of calculations, which predict exactly such reversal of the relative intensity pattern for the 1062 and 1074 cm^{-1} peaks upon going from a planar to a twisted dimeric form (see Figure 6).

3.6. High-Pressure Experiments. The idea behind spectral measurements for samples submitted to high pressures was to observe pressure-induced changes in the strength, and possibly also of the structure of the intermolecular hydrogen bond. Figure 8 shows the Raman spectra recorded for PQ dimers under normal and elevated pressures. Nearly all peaks observed below 1700 cm^{-1} evolve in a similar way with increasing pressure: the maxima shift to the blue by 5–8 cm^{-1}. Much larger shifts towards higher transition energies are detected for the CH stretching bands, which shift by 30 cm^{-1} or more. A reversal of the relative intensities is observed for the bands at 3114 and 3137 cm^{-1}. All these changes are reversible, as shown by comparison of the spectra recorded for the same sample before and after going through the high pressure cycle.

The effects most relevant to this work are related to changes in the HB strength and structure. Figure 8 shows that the NH stretching band, observed at 3200 cm^{-1}, moves to

Table 1: Comparison of the experimental IR and Raman spectra with the vibrational frequencies calculated for the twisted and planar forms of the PQ dimer.

	Calculated[a]						Observed				
	frequency[e] (cm^{-1})	frequency[f] (cm^{-1})	IR intensity[g] (km/mol)		Raman activity[g] (A^4/amu)		IR[b]		Raman[c]		Assignment[d]
							3362				
ν_1	3218.9	3218.8	2578.38	(1802.54)	28.41	(0)	3180[h]	s			as NH str
ν_2	3201.3	3211.2	48.28	(0.01)	1126.68	(1032.01)			3193[h]	s	s NH str
ν_3	3151.3	3065.3	4.97	(7.27)	49.50	(53.58)					as CH str
ν_4	3151.3	3065.3	0.52	(1.43)	281.36	(272.92)			3137	w	s CH str
ν_5	3133.0	3039.3	0.75	(0.64)	164.25	(237.43)			3112	w	s CH str
ν_6	3133.0	3039.3	5.02	(6.87)	39.47	(22.30)					as CH str
ν_7	3091.4	2996.7	4.88	(0.14)	453.54	(555.04)			3067	w	s CH str
ν_8	3091.4	2996.6	29.73	(36.36)	95.36	(2.32)					as CH str
ν_9	3078.3	2983.2	1.61	(0.01)	501.64	(515.94)			3052	w	s CH str
ν_{10}	3078.2	2983.1	63.42	(60.51)	27.11	(0.05)					as CH str
ν_{11}	3062.4	2970.2	0.17	(17.58)	302.47	(121.90)			3040	w	s CH str
ν_{12}	3062.4	2969.9	19.75	(17.35)	24.36	(125.43)					as CH str
ν_{13}	3059.7	2966.6	2.18	(8.51)	2.32	(113.18)					as CH str
ν_{14}	3059.6	2966.4	0.33	(6.59)	12.54	(140.11)			3019	sh	s CH str
ν_{15}	3039.2	2964.5	4.87	(0.27)	148.24	(30.94)			3000		s CH str
ν_{16}	3039.1	2964.5	15.73	(0.38)	28.75	(42.60)					as CH str
							1660	m			
							1632	m			
ν_{17}	1602.8	1551.4	6.25	(0)	50.40	(53.35)			1620	m	NH s b, CC str cr
ν_{18}	1598.7	1548.4	36.68	(27.79)	10.29	(0)	1615	s			NH as b,CC str cr
ν_{19}	1581.1	1534.2	27.87	(34.95)	13.16	(0.07)	1594	m			(CC, CN) as str pyridine
ν_{20}	1580.3	1533.4	4.33	(0.03)	66.13	(81.74)			1595	m	(CC, CN) s str pyridine
ν_{21}	1549.9	1499.8	0.99	(0.01)	28.48	(30.40)			1562	m	NH, CH s b pyridine
ν_{22}	1545.9	1497.7	57.03	(43.42)	6.11	(0.01)	1560	m			NH, CH as b pyridine
ν_{23}	1515.0	1468.1	4.14	(0)	21.16	(27.48)			1528	w	NH, CH18,20,41,39 s b
ν_{24}	1512.5	1466.6	90.78	(95.24)	5.73	(0)	1524	s			NH, CH18,20,41,39 as b
ν_{25}	1488.0	1441.3	40.20	(42.88)	17.42	(0)	1497	m			NH as b, CC str pyr
ν_{26}	1484.3	1436.4	4.55	(0)	111.20	(172.84)			1500	s	NH s b, CC str pyr
ν_{27}	1469.8	1423.5	1.32	(0)	243.81	(225.53)			1484	vs	CH20 s b, skel def CC
ν_{28}	1468.1	1422.0	9.96	(7.03)	56.54	(0)	1482	w			CH20 as b, skel def CC
ν_{29}	1427.9	1385.4	0.77	(0)	37.40	(32.30)			1440	w	NH, CH20,21,41,42 s b, skel def pyr
ν_{30}	1427.2	1379.4	9.25	(10.49)	6.91	(0)	1435	w			NH, CH20,21,41,42 as b, skel def pyr
ν_{31}	1414.9	1369.1	4.96	(6.27)	0.97	(0)	1428	w			CH17,18,19,20,38,39,40,41 as b, CC str cr
ν_{32}	1414.7	1366.9	0.84	(0)	9.32	(13.32)			1430	m	CH17,18,19,20,38,39,40,41 s b, CC str cr
ν_{33}	1394.6	1345.2	0.04	(0)	152.39	(137.61)			1407	m	NH, CH21,42 s b, CC str pyr
ν_{34}	1388.7	1343.6	33.68	(37.34)	17.26	(0.01)	1403	m			NH, CH21,42 as b, CC str pyr,
ν_{35}	1363.7	1318.7	124.83	(146.01)	22.36	(0)	1386	s			skel def, CH as b
ν_{36}	1361.7	1315.9	20.55	(0)	111.09	(157.34)			1386	s	skel def, CH s b
ν_{37}	1324.1	1280.6	6.01	(0)	78.48	(84.13)			1341	m	skel def, CH s b
ν_{38}	1320.2	1277.8	87.62	(85.48)	10.37	(0)	1333	m			skel def, CH as b
ν_{39}	1291.9	1249.4	3.58	(1.30)	32.85	(0.26)	1301	vw			skel def, CH as b
ν_{40}	1291.3	1248.8	0.77	(0)	119.86	(125.70)			1302	m	skel def, CH s b
ν_{41}	1263.8	1225.6	1.51	(0)	13.98	(24.15)			1275	m	CH s b, C7N11, C28N32, C8C9, C29C30 str
ν_{42}	1263.4	1222.7	37.25	(32.35)	1.74	(0)	1268	m			CH as b, C7N11, C28N32, C8C9, C29C30 str

Table 1: Continued.

	Calculated[a]						Observed				
	frequency[e] (cm^{-1})	frequency[f] (cm^{-1})	IR intensity[g] (km/mol)		Raman activity[g] (A^4/amu)		IR[b]		Raman[c]		Assignment[d]
ν_{43}	1239.0	1199.9	1.23	(24.33)	2.28	(0.02)			1251	w	NH and CH s b
ν_{44}	1236.5	1199.8	24.70	(0.11)	0.43	(4.81)	1243	m			NH and CH as b
ν_{45}	1199.6	1160.3	1.67	(0.57)	0.25	(0)	1210	w			CH as b, CC str cr
ν_{46}	1199.5	1159.7	0.03	(0)	1.27	(1.08)			1210	w	CH s b, CC str cr
ν_{47}	1180.7	1140.7	0.58	(16.59)	2.52	(0)			1193	w	CH s b, CC str
ν_{48}	1180.6	1138.8	15.28	(0)	0.09	(2.07)	1193	m			CH s b, CC str
ν_{49}	1123.7	1089.2	8.81	(10.81)	0.66	(0.01)	1133	m			CH17,18,19,20 and CH38,39,40,41 as b
ν_{50}	1123.5	1089.1	1.71	(0.03)	2.24	(2.15)			1132	w	CH17,18,19,20 and CH38,39,40,41 s b
ν_{51}	1112.3	1074.6	0.50	(25.90)	1.01	(0)					CH15,17,18,20 and CH36,38,39,41 and NH s b
ν_{52}	1110.6	1074.1	22.51	(0)	0.23	(4.96)	1121	m			CH15,17,18,20 and CH36,38,39,41 and NH as b
ν_{53}	1075.6	1041.7	0.14	(0)	3.42	(8.06)			1090	w	skel def, CH s b
ν_{54}	1071.0	1035.3	51.41	(69.84)	0.35	(0)	1082	s			skel def, CH as b
ν_{55}	1056.8	1026.7	0.02	(0)	30.98	(69.48)			1075	s	CH15,16,36,37 s b
ν_{56}	1055.9	1024.6	4.03	(3.50)	2.00	(0)	1065	w			CH15,16,36,37 s b
ν_{57}	1047.8	1015.9	0.86	(0)	53.49	(21.34)			1062	m	skel def, CH as b
ν_{58}	1046.4	1012.3	5.31	(11.68)	2.32	(0)	1058	w			skel def, CH as b
ν_{59}	1008.9	978.5	5.64	(6.69)	3.18	(0)	1025	w			skel def
ν_{60}	1008.6	975.5	0.60	(0)	24.42	(17.84)			1019	w	skel def
ν_{61}	968.6	931.8	1.25	(1.27)	0.15	(0)	972	vw	973	vw	CH19-21 and CH40-42 s “oop” twisting
ν_{62}	968.6	931.7	0.32	(0)	0.04	(0.24)	965	vw	969	vw	CH19-21 and CH40-42 as “oop” twisting
ν_{63}	944.2	909.4	0.03	(0)	0.26	(0.60)			951	w	CH17,18,21 and CH38,39,42 as “oop” wag
ν_{64}	944.1	909.4	0.11	(0.38)	0.13	(0)					CH17,18,21 and CH38,39,42 as “oop” wag
ν_{65}	938.9	887.5	0.86	(1.71)	0.40	(0.11)	946	w			CH17-19,21 and CH38-40,42 as “oop” twisting
ν_{66}	938.8	887.3	0.76	(0.28)	0.41	(0.66)			942	w	CH17-19,21 and CH38-40,42 as “oop” twisting
ν_{67}	888.4	857.1	51.13	(44.91)	2.84	(0)	899	m			as skel def pyr (N11-C12-C13)
ν_{68}	885.0	851.4	16.47	(0)	26.78	(25.25)			890	m	s skel def pyr (N11-C12-C13)
ν_{69}	872.9	841.8	10.51	(17.27)	4.86	(0)	882	m			skel def, NH s twisting
ν_{70}	871.3	839.8	16.74	(0)	1.46	(20.52)					skel def, NH as twisting
ν_{71}	860.9	809.0	9.07	(0)	13.06	(0.03)			853	w	CH15,16,36,37 and s “oop” wag
ν_{72}	857.2	808.8	2.82	(21.39)	0.83	(0)	860	vw			CH15,16,36,37 and s “oop” wag
ν_{73}	829.1	793.1	1.31	(43.69)	0.63	(0)					s skel “oop” def, NH, CH wag
ν_{74}	823.8	789.6	5.18	(0)	0.65	(1.24)					as skel “oop” def, NH, CH wag
ν_{75}	814.6	774.0	103.69	(76.52)	2.72	(0)	823	m	826	w	s NH “oop”
ν_{76}	805.0	771.8	9.08	(0)	0.45	(0.73)					as cr “oop” def, CH as wag
ν_{77}	804.3	735.0	29.08	(0)	0.76	(0.29)	801	s			s cr “oop” def, CH s wag
ν_{78}	782.9	733.5	5.92	(33.11)	0.03	(0)					as NH “oop”
ν_{79}	764.2	728.2	5.35	(0)	0.23	(32.85)					CH17-21,38-42 s “oop” wag
ν_{80}	763.1	727.2	0.29	(2.50)	0.05	(0)					CH17-21,38-42 s “oop” wag
ν_{81}	751.2	716.8	1.01	(57.55)	36.36	(0)			763	m	s “ip” skel def
ν_{82}	750.8	699.1	1.33	(0)	3.39	(0.26)	773	m	770	sh	as “ip” skel def
ν_{83}	727.8	688.3	17.14	(1.95)	0.14	(0)	738	m	739	w	CH15-18 and CH36-39 “oop” s wag
ν_{84}	726.3	669.7	2.58	(65.15)	0.02	(0)					CH15-18 and CH36-39 “oop” as wag
ν_{85}	696.2	668.3	61.18	(0)	1.87	(0.88)					s “oop” skel def, CH s wag
ν_{86}	696.1	656.9	13.35	(0)	0.05	(0.71)					as “oop” skel def, CH s wag

Table 1: Continued.

	Calculated[a]						Observed				
	frequency[e] (cm^{-1})	frequency[f] (cm^{-1})	IR intensity[g] (km/mol)		Raman activity[g] (A^4/amu)		IR[b]		Raman[c]		Assignment[d]
ν_{87}	678.6	653.4	0.03	(0)	64.70	(70.42)	684	vw	686	s	s cr and pyridine ring b (sym along N1-C4, C7-C10 axis)
ν_{88}	675.2	651.1	15.94	(14.61)	1.87	(0)	696	m	696	sh	as cr and pyridine ring b (sym along N1-C4, C7-C10 axis)
ν_{89}	610.6	589.1	5.28	(4.30)	0.01	(0)					as cr and pyridine ring b (asym along N1-C4, C7-C10 axis)
ν_{90}	607.0	587.8	1.15	(0)	6.13	(8.11)	615	vw	614	w	s cr and pyridine ring b (asym along N1-C4, C7-C10 axis)
ν_{91}	605.3	575.9	0.89	(14.68)	0.58	(0)					as "oop" skel def pyr
ν_{92}	604.5	572.2	6.17	(0)	2.14	(0.68)			602	w	s "oop" skel def pyr
ν_{93}	573.7	552.4	0.75	(2.39)	0.53	(0)					as "oop" skel def pyridine and cr
ν_{94}	573.5	547.6	0.55	(0)	0.98	(2.04)			571	w	s "oop" skel def pyridine and cr
ν_{95}	516.2	502.9	5.97	(7.19)	1.51	(0)					as "ip" skel def pyridine and cr
ν_{96}	516.1	500.6	0.74	(0)	8.04	(10.89)			524	m	s "ip" skel def pyridine and cr
ν_{97}	513.7	490.9	0.53	(0)	1.51	(1.03)			513	w	s "oop" skel def pyridine and cr
ν_{98}	511.6	485.2	0.17	(0.81)	0.72	(0)					as "oop" skel def pyridine and cr
ν_{99}	472.8	455.0	8.28	(0)	1.82	(9.13)					as "ip" skel def cr
ν_{100}	471.5	453.5	0.17	(8.39)	8.11	(0)			479	m	s "ip" skel def cr
ν_{101}	430.1	414.5	0.54	(8.03)	11.61	(0)			438	m	s "ip" skel def cr, CH17,19,38,40 "oop"
ν_{102}	429.9	414.3	7.54	(0)	2.59	(15.89)			432	sh	as "ip" skel def cr, CH17,19,38,40 "oop"
ν_{103}	426.3	411.4	0.52	(0)	1.64	(2.25)					as "oop" skel def cr, CH17,19,38,40 "oop"
ν_{104}	425.1	410.3	0.58	(2.00)	4.49	(0)			424	w	s "oop" skel def cr, CH17,19,38,40 "oop"
ν_{105}	284.4	273.3	1.89	(1.93)	0.81	(0)					as "oop" pyridine and cr rock
ν_{106}	283.5	270.9	1.37	(0)	1.34	(2.06)			300	w	s "oop" pyridine and cr rock
ν_{107}	252.8	244.7	0.65	(6.73)	0.04	(0)					as "oop" pyr and cr rock
ν_{108}	249.5	238.0	6.20	(6.29)	0.17	(0)					s "oop" pyr and cr rock
ν_{109}	248.8	237.5	3.53	(0)	0.52	(6.82)			267	w	as pyr and pyridine rings "ip" bend
ν_{110}	243.3	231.8	0.07	(0)	5.18	(0.05)			251	m	s pyr and pyridine rings "ip" bend
ν_{111}	163.0	141.8	0.01	(0.04)	0.27	(0)			169	w	as pyr and pyridine tor
ν_{112}	150.4	139.1	0.03	(0)	0.43	(1.24)			154	m	s pyr and pyridine tor
ν_{113}	122.3	117.0	6.27	(0)	0.23	(2.44)					as "oop" pyridine and pyr rock
ν_{114}	121.9	112.3	3.70	(6.00)	0.91	(0)					s "oop" pyridine and pyr rock
ν_{115}	80.2	75.9	3.58	(1.02)	3.54	(0)					dim rock
ν_{116}	78.2	71.4	0.02	(0)	1.54	(1.80)					dim b
ν_{117}	67.0	59.6	0.00	(0)	1.15	(3.12)					dim b
ν_{118}	43.4	21.3	0.18	(0.12)	9.82	(0)					dim rock
ν_{119}	26.1	9.2	0.27	(0)	4.96	(15.09)					dim rock
ν_{120}	21.3	−35.3	0.04	(0)	11.69	(0)					dim tor

[a]B3LYP/cc-pVTZ, C_2 symmetry group, scaling factor = 0.9682, as recommended in the literature [39].
[b]Polycrystalline sample, 293 K.
[c]Polycrystalline sample, 293 K, 785 nm laser (633 nm was used in the NH region).
[d]Abbreviations. s: symmetric; as: antisymmetric; str: stretch; b: bend; ip: in-plane; oop: out-of-plane; skel def: skeletal deformation; tor: torsion; pyrid: pyridine; pyr: pyrrole; cr: central ring.
[e]Twisted dimer.
[f]Planar dimer.
[g]In parentheses: values computed for the planar dimer.
[h]Very broad (~200 cm^{-1}).

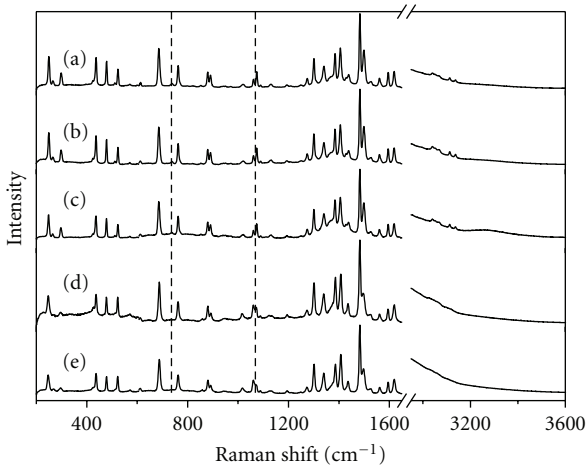

FIGURE 7: Raman spectra measured for samples crystallized from five different solvents: cyclohexane (a), methanol (b), toluene (c), dichloromethane (d), diethyl ether (e). Dashed vertical lines indicate regions with structure-sensitive transitions (see text).

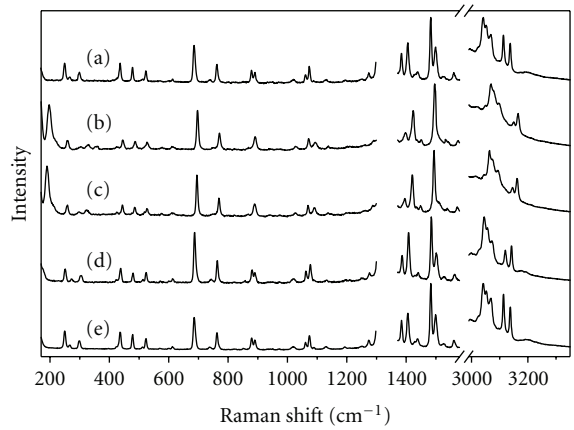

FIGURE 8: Raman spectra of crystalline PQ as a function of pressure: normal pressure, 1 atm (a); 2×10^3 atm (b); 22×10^3 atm (c); 35×10^3 atm (d); 1 atm (e), at the end of pressure cycle. The low and high frequency regions are normalized separately to their highest bands. A region between 1300–1370 cm^{-1}, exhibiting a strong Raman peak from diamond culets, was removed.

the red with increasing pressure. Such behavior is opposite to that of other modes and indicates the increase of the HB strength, most probably due to a shorter NH$\cdots$N distance. Unfortunately, the exact amount of the shift cannot be determined, as the band becomes buried under the transitions corresponding to CH stretches. Experiments are planned with either N- or C-deuterated PQ, to avoid interferences of NH/ND vibrations with other modes.

The second effect is the change in the relative intensity pattern with increasing pressure, observed for the peaks at 1062 and 1074 cm^{-1}. As discussed above, such behaviour can indicate a transition from a cyclic toward a twisted structure. For another mode diagnostic in this respect, 738 cm^{-1}, we observe decreasing intensity. However, it can still be detected at the highest pressures applied. It may be that what is

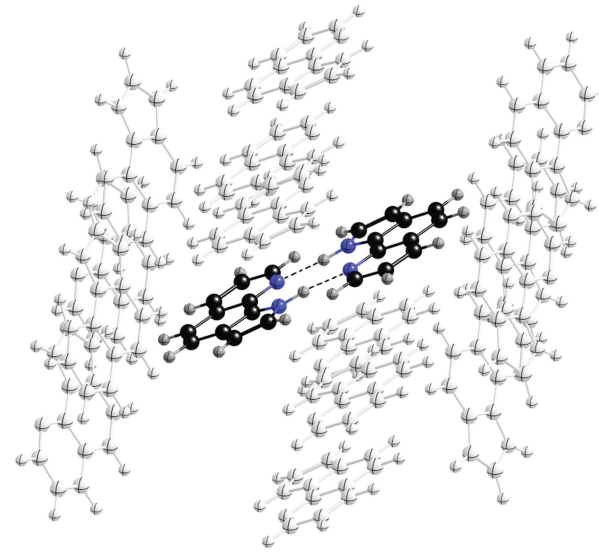

FIGURE 9: PQ dimer surrounded by identical neighbors (taken from X-ray data). The dimer in the middle was being distorted along the twisting coordinate, and then the whole structure was optimized.

observed is gradual twisting, not necessarily leading to the same angle between the monomeric units as observed for the nonplanar polymorph under normal pressure. More detailed investigations are planned once both planar and twisted dimeric samples are available. The experiments described in the previous section bode well for such studies.

3.7. Simulations of Polymorphic Structures. The existence of both planar and twisted dimers leads to the question of the energy barrier separating the two phases. Theoretical simulations have been carried out, in order to check the local minimum character of each structure and to estimate their relative stabilities. In this procedure, a dimer, surrounded by 14 identical neighbours (Figure 9), was distorted towards the structure of the other polymorph (twisted for the initially planar form, and vice versa). The whole ensemble was then optimized. Both planar and twisted structures relaxed back to the initial form, showing that they correspond to the minimum and providing additional independent confirmation of the existence of two crystal polymorphic forms of the PQ dimer. These results indicate that a collective rather than local distortion of the crystal is required for the phase change in PQ.

In agreement with the high pressure experiments, comparison of energies calculated for the slab consisting of 16 molecules for both planar and twisted dimers revealed a lower energy for the latter.

4. Summary and Conclusions

A combination of X-ray, IR and Raman spectroscopy, high pressure techniques, and quantum chemical calculations resulted in the detection of two polymorphic forms of dimeric PQ. Both types of dimer reveal a cyclic, doubly

hydrogen-bonded structure, but differ in the planar versus twisted arrangement of the monomeric units. The calculations predict a twisted dimer structure, whereas imposing planarity results in one negative vibrational frequency, corresponding to the twisting coordinate. These results show that the isolated dimer should be nonplanar and thus the polymorphism is due to the interplay of interactions between the two monomeric units forming the hydrogen bond and dimer-dimer interactions in the crystal. The experiments indicate that upon applying pressure the planar form can be converted into the twisted one.

The NH stretching and out-of-plane bending modes observed in the IR spectra were shown to be clear indicators of the HB formation. The analysis of the position of the latter could be used to determine the structure of the H-bonded dimer. With respect to the influence of HB formation on the Raman spectra, a large increase of the intensity was observed for the NH stretching band in the H-bonded dimers, indicating increase of polarizability. The Raman spectra were also diagnostic for structural assignments: even though the spectra are quite similar, the intensity ratio of two peaks observed at 1062 and 1074 cm^{-1} provides information whether the PQ dimer is planar or not.

Our future plans include testing a possibility of photoinduced double proton transfer in both forms of crystalline PQ. Both kinetics and thermodynamics of such a process should be strongly structure-sensitive. Moreover, we have selected PQ as one of the objects in the investigations of the influence of plasmonic structures on the spectral and photophysical characteristics of chromophores located in the vicinity of metallic environments. The results of vibrational and structural analysis presented in this work will provide a starting point for experiments in which monomers and dimers of PQ will be placed on, or close to metal surfaces.

Acknowledgments

The work was supported by the Grant 3550/B/H03/2011/40 from the Polish National Science Centre. The authors acknowledge the computing grant G17-14 from the Interdisciplinary Centre for Mathematical and Computational Modeling of the Warsaw University. They would like to thank bwGRiD (http://www.bw-grid.de), member of the German D-Grid initiative, funded by the Ministry for Education and Research (Bundesministerium für Bildung und Forschung) and the Ministry for Science, Research and Arts Baden-Württemberg (Ministerium für Wissenschaft, Forschung und Kunst Baden-Württemberg), for providing the opportunity to use parallel computing facilities and perform quantum chemical calculations. R. P. Thummel thanks the Robert A. Welch Foundation (E-621) and the National Science Foundation (CHE-0714751).

References

[1] J. Waluk, "Hydrogen-bonding-induced phenomena in bifunctional heteroazaaromatics," *Accounts of Chemical Research*, vol. 36, no. 11, pp. 832–838, 2003.

[2] J. A. Walmsley, "Self-association of 7-azaindole in nonpolar solvents," *The Journal of Physical Chemistry*, vol. 85, no. 21, pp. 3181–3187, 1981.

[3] P. Dufour, Y. Dartiguenave, M. Dartiguenave et al., "Crystal structures of 7-azaindole, an unusual hydrogen-bonded tetramer, and of two of its methylmercury(II)complexes," *Canadian Journal of Chemistry*, vol. 68, no. 1, pp. 193–201, 1990.

[4] H. Yokoyama, H. Watanabe, T. Omi, S. I. Ishiuchi, and M. Fujii, "Structure of hydrogen-bonded clusters of 7-azaindole studied by IR dip spectroscopy and ab initio molecular orbital calculation," *Journal of Physical Chemistry A*, vol. 105, no. 41, pp. 9366–9374, 2001.

[5] K. Sakota, Y. Kageura, and H. Sekiya, "Cooperativity of hydrogen-bonded networks in 7-azaindole$(CH_3OH)_n$ ($n = 2, 3$)clusters evidenced by IR-UV ion-dip spectroscopy and natural bond orbital analysis," *Journal of Chemical Physics*, vol. 129, no. 5, Article ID 054303, 2008.

[6] K. Sakota, Y. Komure, W. Ishikawa, and H. Sekiya, "Spectroscopic study on the structural isomers of 7-azaindole(ethanol)$_n$ ($n = 1 - 3$) and multiple-proton transfer reactions in the gas phase," *Journal of Chemical Physics*, vol. 130, no. 22, Article ID 224307, 2009.

[7] T. B. C. Vu, I. Kalkman, W. L. Meerts, Y. N. Svartsov, C. Jacoby, and M. Schmitt, "Rotationally resolved electronic spectroscopy of water clusters of 7-azaindole," *Journal of Chemical Physics*, vol. 128, no. 21, Article ID 214311, 2008.

[8] G. A. Pino, I. Alata, C. Dedonder, C. Jouvet, K. Sakota, and H. Sekiya, "Photon induced isomerization in the first excited state of the 7-azaindole-$(H_2O)_3$ cluster," *Physical Chemistry Chemical Physics*, vol. 13, no. 13, pp. 6325–6331, 2011.

[9] K. Sakota, C. Jouvet, C. Dedonder, M. Fujii, and H. Sekiya, "Excited-state triple-proton transfer in 7-azaindole$(H_2O)_2$ and reaction path studied by electronic spectroscopy in the gas phase and quantum chemical calculations," *Journal of Physical Chemistry A*, vol. 114, no. 42, pp. 11161–11166, 2010.

[10] K. Suwińska, "Crystal structure communications," *Acta Crystallographica C*, vol. 41, pp. 973–975, 1985.

[11] J. Waluk and B. Pakuła, "Viscosity and temperature effects in excited state double proton transfer: iuminescence of 1-azacarbazole dimers in solid state and solution," *Journal of Molecular Structure*, vol. 114, pp. 359–362, 1984.

[12] J. Waluk, A. Grabowska, B. Pakuła, and J. Sepioł, "Viscosity vs. temperature effects in excited-state double proton transfer. Comparison of 1-azacarbazole with 7-azaindole," *The Journal of Physical Chemistry*, vol. 88, no. 6, pp. 1160–1162, 1984.

[13] J. Waluk, J. Herbich, D. Oelkrug, and S. Uhl, "Excited-state double proton transfer in the solid state: the dimers of 1-azacarbazole," *Journal of Physical Chemistry*, vol. 90, no. 17, pp. 3866–3868, 1986.

[14] J. Catalán, "Photophysics of 1-azacarbazole dimers: a reappraisal," *The Journal of Physical Chemistry A*, vol. 111, no. 36, pp. 8774–8779, 2007.

[15] D. Marks, H. Zhang, P. Borowicz, J. Waluk, and M. Glasbeek, "(Sub)picosecond fluorescence upconversion studies of intermolecular proton transfer of dipyrido[2,3-a:3′,2′-i]carbazole and related compounds," *Journal of Physical Chemistry A*, vol. 104, no. 31, pp. 7167–7175, 2000.

[16] A. Kyrychenko, J. Herbich, M. Izydorzak, F. Wu, R. P. Thummel, and J. Waluk, "Role of ground state structure in photoinduced tautomerization in bifunctional proton donor-acceptor molecules: 1H-pyrrolo[3,2-*h*]quinoline and related

compounds," *Journal of the American Chemical Society*, vol. 121, no. 48, pp. 11179–11188, 1999.

[17] A. Kyrychenko and J. Waluk, "Excited-state proton transfer through water bridges and structure of hydrogen-bonded complexes in 1H-pyrrolo[3,2-*h*]quinoline: adiabatic time-dependent density functional theory study," *The Journal of Physical Chemistry A*, vol. 110, no. 43, pp. 11958–11967, 2006.

[18] Y. Nosenko, M. Kunitski, R. P. Thummel et al., "Detection and structural characterization of clusters with ultrashort-lived electronically excited states: IR absorption detected by femtosecond multiphoton ionization," *Journal of the American Chemical Society*, vol. 128, no. 31, pp. 10000–10001, 2006.

[19] Y. Nosenko, A. Kyrychenko, R. P. Thummel, J. Waluk, B. Brutschy, and J. Herbich, "Fluorescence quenching in cyclic hydrogen-bonded complexes of 1H-pyrrolo[3,2-*h*]quinoline with methanol: cluster size effect," *Physical Chemistry Chemical Physics*, vol. 9, no. 25, pp. 3276–3285, 2007.

[20] Y. Nosenko, M. Kunitski, C. Riehn et al., "Separation of different hydrogen-bonded clusters by femtosecond UV-ionization-detected infrared spectroscopy: 1H-pyrrolo[3,2-*h*] quinoline$\cdot(H_2O)_{n=1,2}$ complexes," *Journal of Physical Chemistry A*, vol. 112, no. 6, pp. 1150–1156, 2008.

[21] J. Herbich, J. Sepioł, and J. Waluk, "Determination of the energy barrier origin of the excited state double proton transfer in 7-azaindole: alcohol complexes," *Journal of Molecular Structure*, vol. 114, pp. 329–332, 1984.

[22] D. McMorrow and T. J. Aartsma, "Solvent-mediated proton transfer. The roles of solvent structure and dynamics on the excited-state tautomerization of 7-azaindole/alcohol complexes," *Chemical Physics Letters*, vol. 125, no. 5-6, pp. 581–585, 1986.

[23] J. Konijnenberg, A. H. Huizer, and C. A. G. O. Varma, "Solute-solvent interaction in the photoinduced tautomerization of 7-azaindole in various alcohols and in mixtures of cyclohexane and ethanol," *Journal of the Chemical Society, Faraday Transactions 2*, vol. 84, no. 8, pp. 1163–1175, 1988.

[24] R. S. Moog, S. C. Bovino, and J. D. Simon, "Solvent relaxation and excited-state proton transfer: 7-azaindole in ethanol," *Journal of Physical Chemistry*, vol. 92, no. 23, pp. 6545–6547, 1988.

[25] R. S. Moog and M. Maroncelli, "7-Azaindole in alcohols: solvation dynamics and proton transfer," *Journal of Physical Chemistry*, vol. 95, no. 25, pp. 10359–10369, 1991.

[26] A. V. Smirnov, D. S. English, R. L. Rich et al., "Photophysics and biological applications of 7-azaindole and its analogs," *Journal of Physical Chemistry B*, vol. 101, no. 15, pp. 2758–2769, 1997.

[27] S. Mente and M. Maroncelli, "Solvation and the excited-state tautomerization of 7-azaindole and 1-azacarbazole: computer simulations in water and alcohol solvents," *Journal of Physical Chemistry A*, vol. 102, no. 22, pp. 3860–3876, 1998.

[28] K. C. Ingham, M. Abu-Elgheit, and M. Ashraf El-Bayoumi, "Confirmation of biprotonic phototautomerism in 7-azaindole hydrogen-bonded dimers," *Journal of the American Chemical Society*, vol. 93, no. 20, pp. 5023–5025, 1971.

[29] S. N. Krasnokutskii, L. N. Kurkovskaya, T. A. Shibanova, and V. P. Shabunova, "Structure of 1H-pyrrolo[3,2-*h*]quinoline," *Zhurnal Strukturnoi Khimii*, vol. 32, p. 131, 1991.

[30] J. Herbich, M. Kijak, R. Luboradzki et al., "In search for phototautomerization in solid dipyrido[2,3-a:3′,2′-i]carbazole ," *Journal of Photochemistry and Photobiology A*, vol. 154, no. 1, pp. 61–68, 2002.

[31] F. Wu, C. M. Chamchoumis, and R. P. Thummel, "Bidentate ligands that contain pyrrole in place of pyridine," *Inorganic Chemistry*, vol. 39, no. 3, pp. 584–590, 2000.

[32] K. Takemura, S. Minomura, O. Shimomura, and Y. Fujii, "Observation of molecular dissociation of iodine at high pressure by X-ray diffraction," *Physical Review Letters*, vol. 45, no. 23, pp. 1881–1884, 1980.

[33] H. K. Mao, P. M. Bell, J. W. Shaner, and D. J. Steiberg, "Specific volume measurements of Cu, Mo, Pd, and Ag and calibration of the ruby R_1 fluorescence pressure gauge from 0.06 to 1 Mbar," *Journal of Applied Physics*, vol. 49, no. 6, pp. 3276–3283, 1978.

[34] G. M. Sheldrick, "Foundations of crystallography," *Acta Crystallographica A*, vol. 64, pp. 112–122, 2008.

[35] M. D. Segall, P. J. D. Lindan, M. J. Probert et al., "First-principles simulation: ideas, illustrations and the CASTEP code," *Journal of Physics Condensed Matter*, vol. 14, no. 11, pp. 2717–2744, 2002.

[36] J. P. Perdew, J. A. Chevary, S. H. Vosko et al., "Atoms, molecules, solids, and surfaces: applications of the generalized gradient approximation for exchange and correlation," *Physical Review B*, vol. 46, no. 11, pp. 6671–6687, 1992.

[37] D. Vanderbilt, "Soft self-consistent pseudopotentials in a generalized eigenvalue formalism," *Physical Review B*, vol. 41, no. 11, pp. 7892–7895, 1990.

[38] H. J. Monkhorst and J. D. Pack, "Special points for Brillouin-zone integrations," *Physical Review B*, vol. 13, no. 12, pp. 5188–5192, 1976.

[39] J. P. Merrick, D. Moran, and L. Radom, "An evaluation of harmonic vibrational frequency scale factors," *Journal of Physical Chemistry A*, vol. 111, no. 45, pp. 11683–11700, 2007.